Precipitation Growth Processes in the Comma Head Region of the 7 February 2020 Snowstorm observed during IMPACTS

Megan M. Varcie[1], Troy J. Zaremba[1] , Robert M. Rauber[1], Greg M. McFarquhar[2,3], Joseph A. Finlon[4], Lynn A. McMurdie[4], and Alexander V. Ryzhkov[2,5]

[1]Department of Atmospheric Sciences, University of Illinois Urbana-Champaign; [2]Cooperative Institute for Mesoscale Meteorological Studies, University of Oklahoma
[3]School of Meteorology, University of Oklahoma; [4]Department of Atmospheric Sciences, University of Washington;
[5]NOAA/OAR National Severe Storms Laboratory

Motivation

Increasing interest in dynamic cloud-top substructures, lack of in-situ microphysical observations aloft to characterize these dynamic features, and numerous recent high-impact winter storms along the East Coast culminated as motivation for the Investigation of Microphysics and Precipitation for Atlantic Coast Threatening Snowstorms (IMPACTS) field campaign. The 7 February 2020 event, in addition to being the most well-coordinated mission of the 2020 deployment, was a favorable winter storm for analysis as it was characterized by stratiform and convective regions in the horizontal plane, the latter forming as a result of superposition of two airmasses, one below and one above the warm front. This case study will analyze how microphysics evolve as particles descend through different particle growth layers when generating cells were and were not present at cloud top. This study will also analyze the physical mechanisms for particle growth through specified layers.

7 February 2020 Sampling Strategy

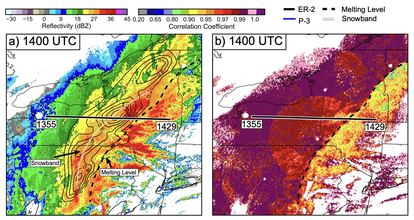

The NASA ER-2 and P-3 Orion collected remote sensing and in situ microphysics data within the comma head region of the 7 February 2020 snowstorm over Central New York on 7 February 2020. Fig. 1 above shows WSR-88D reflectivity and correlation coefficient within the comma head at 2.5 km overlaid with 700 mb kinematic frontogenesis valid at 14 UTC from RAP analysis. A broad snowband was sampled by both aircraft over central New York which was collocated with the axis of maximum 700 mb frontogenesis. The rain snow line, and resulting bright band effects, bisected the aircraft track at 2.5 km as evidenced by the reduction in the correlation coefficient over Eastern New York.

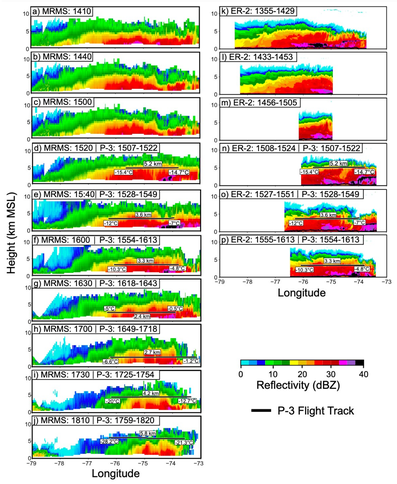

During the 7 February 2020 research flights, the ER-2 aircraft was operational from 1400 to 1600 UTC and completed six total flight legs at an altitude of ~20 km. The P-3 was operational from 1500 to 1800 UTC completing seven total flight legs. The P-3 flight legs were completed at varying altitudes between 2 and 6 km at temperatures between -27°C and 0°C. Three flight legs were coordinated between the ER-2 and P-3 followed by four additional P-3 flight legs after the ER-2 returned to base. Fig. 2d-j shows the location of the P-3 overlaid on MRMS cross sections of reflectivity and Fig. 2n-p show the location of the P-3 overlaid over EXRAD reflectivity.

7 February 2020 Thermodynamic Properties

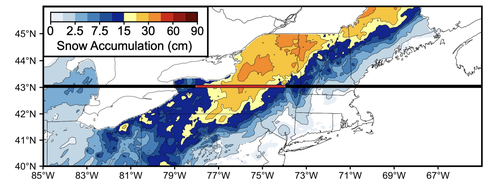

Fig. 3 shows surface snowfall accumulations across central New York. Accumulations of 20-30 cm (7.8-11.8 in) fell by 0000 UTC on 8 February. In order to characterize the thermodynamic environment influencing the comma head region of the 7 February 2020 snowstorm, cross sections were created to examine forcing for updrafts responsible for generating cells and banded features. The black line in Fig. 3 shows the location of the cross section in Fig. 4, and the red line in Fig. 3 shows the location of the cross section in Fig. 5.

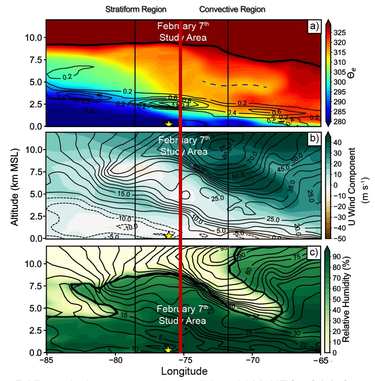

Fig. 4 shows a RAP analysis cross section valid at 1400 UTC of (a) θ_e overlaid with kinematic frontogenesis (°C 100 km^{-1} 3 hr^{-1}), (b) the *u* component of the wind (shaded) and *v* component of the wind (contoured), and (c) relative humidity with respect to water overlaid with total wind speed. The vertical lines denote the east and west flight boundaries. There were two distinct dynamic regimes denoted by the red line above: a stratiform region west of -75.25°W and a convective region east of -75.25°W. These two regions are more evident in Fig. 5.

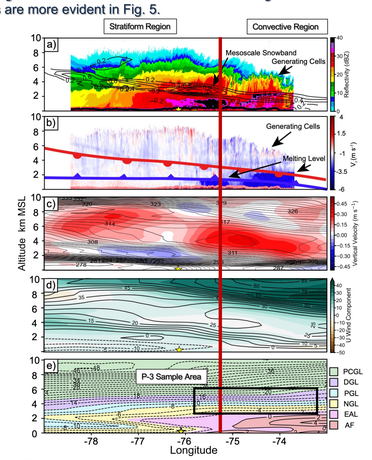

Fig. 5 shows (a) EXRAD reflectivity overlaid with kinematic frontogenesis (°C 100 km^{-1} 3 hr^{-1}) with a maxima over the location of the broad mesoscale snowband (Fig. 1), (b) vertical radial velocity measured by the CRS, (c) RAP analysis vertical velocity capturing the synoptic ascent above the warm front, (d) the cross section parallel component of the wind (shaded) and perpendicular component (contoured), (e) particle growth layers based on temperatures sampled by the P-3: the polycrystalline growth layer (*PCGL; T< -18*°C), the dendritic growth layer (*DGL; -12*°C < T< *-18*°C), the plate growth layer (*PGL; -12*°C < T< -8°C), the needle growth layer (*NGL; -8*°C < T < *-3*°C), the enhanced aggregation layer (*EAL; -3*°C < T< *0*°C), and the above freezing layer (*AF; T > 0*°C). Generating cells formed along the eastern third of the cross section as a result of potential instability due to air ascending both below and above the warm front. These shallow convective updrafts were 1-3 km in depth, exhibited updrafts on the order of 1-3 m s^{-1} and were located above a warm frontal boundary in a potentially unstable layer. The remainder of this analysis will focus on how microphysical processes differed in the stratiform and convective regions of the storm.

Microphysical Characteristics of Growth Layers

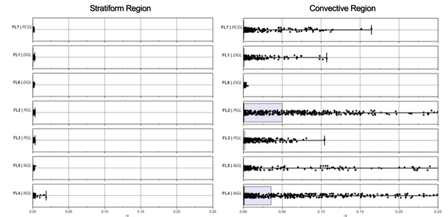

Fig. 6 shows box and whisker CDP supercooled liquid water concentrations (g m^{-3}) for the stratiform region (left) and convective region (right). Box and whisker plots are ordered based on descending temperature layer (*PCGL*, *DGL*, *PGL*, *NGL*). Whiskers represent the extreme values, the box represents the 25th and 75th percentiles, and the black line represents the median value. Each dot represents a 1 Hz measurement. Only trace amounts of SLW were observed in the stratiform region of the storm with the exception of the *NGL*. The stratiform region was devoid of SLW and riming was an unimportant growth process. SLW was much more prevalent in the convective region when compared to the stratiform region. Updrafts were stronger in the convective region evidenced as a result of increased potential instability. SLW was observed in the *PCGL*, *DGL*, *PGL*, and *NGL*. The increase in SLW presence on the east side of the storm led to enhanced particle nucleation, larger number concentrations, enhanced particle growth, and a greater range of particle habits.

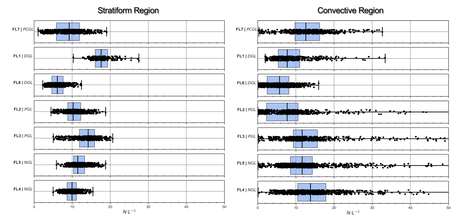

Fig. 7 is the same as Fig. 6 except for total number concentration. Total number concentration was larger in the *PCGL* of the convective region. In the stratiform region, ice crystals primarily nucleated at the top of the *PCGL*. As ice crystals fell through subsequent particle growth layers, they grew by vapor depositional growth which was quantitatively determined by increases in mass and aggregation quantitatively supported by decreases in total number concentration. In the convective region, there was a decrease in total number concentration between the *PCGL* and the *PGL* consistent with particle growth by aggregation. In warmer temperature layers including the *NGL* secondary ice production contributed to the increase in total number concentrations.

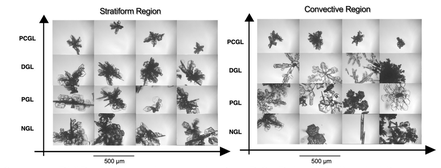

Fig. 8 shows PHIPs images observed by the P-3. Polycrystalline habits were observed through the depth of cloud through all particle growth layers in the stratiform region with no evidence for new particle formation. In the convective region polycrystalline habits were dominant at cloud top. Dendrites formed as pristine crystals in the *DGL* and plates in the *PGL*. Needles were also present in the *NGL* along with rimed particles. These data together with Figs. 6 and 7 suggest that new particle formation occurred throughout the depth of the cloud either by primary nucleation or secondary ice formation processes.

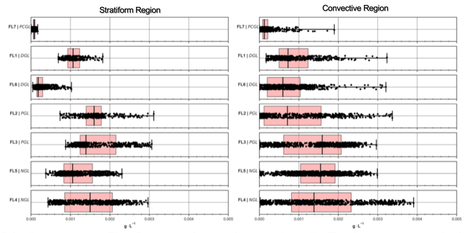

Fig. 9 is the same as Fig. 6 except for total mass (g m^{-3}). Total mass was calculated using habit-specific mass-diameter relationships following McFarquhar et al. (2002). In the stratiform region, mass increased through subsequent particle growth layers, consistent with vapor depositional growth as particles fell through different growth layers. In the convective region, particle mass continually increased with depth with somewhat larger range of masses in the *NGL* compared to the stratiform region. The *NGL* in the convective region had lower median mass likely reflective of the formation of additional smaller and lower mass particles rather than decreasing mass within existing particles.

Nature of the Precipitation Band

Fig. 1 showed two bands of higher reflectivity at 2.5 km associated with comma head. The first appeared directly along and ahead of boundary between the high and low values of the correlation coefficient. The high reflectivity in this region is consistent with melting of ice particles in the radar bright band.

The second band was within the 2.5 km region of high correlation coefficient, indicating ice, and aligned with the axis of maximum 700 mb kinematic frontogenesis suggesting that vertical circulations associated with frontogenesis might be important. However, the cross section in Fig. 5 shows that the high reflectivity associated with the band was confined to altitudes below the region of maximum frontogenesis. A key to understanding the nature of this band appears in Fig. 5b where the high reflectivites are collocated with larger downward radial velocities consistent with values in the melting layer further to the east. These radial velocities suggest that the particles producing the high reflectivity are melted or partially melting and were likely large wet snowflakes. Unfortunately, the P-3 was unable to fly low enough to sample this region.

Conclusions

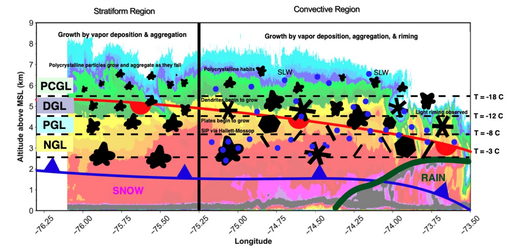

This study quantitatively analyzes the microphysical contrasts between the stratiform and convective regions within the comma head region of a northeast winter cyclone and the influence of cloud top generating cells on the evolution of particles as they descend through different particle growth layers (determined by temperature).

Fig. 10 summarizes the differences between the stratiform and convective regions. In the stratiform region, ice crystals primarily nucleated in the polycrystalline growth layer near cloud top and grew by vapor depositional growth to the ground, which was supported by increases in mass and decreases in total number concentration, consistent with aggregation of the spatially dendritic polycrystalline crystals.

In the convective region, updrafts were on the order of 1-3 m s^{-1} and SLW was abundant throughout the cloud layer, supporting riming, and rapid vapor depositional growth, which resulted in many different particle habits. The bases of cloud top generating cells and associated updrafts were located above the warm front near cloud top and within and above the *DGL*. This created water saturated conditions that allowed for the formation of dendrites and other particles. Pristine crystals also formed in the *PGL*. Conditions for secondary ice production via either the Hallett-Mossop process or droplet shattering were present in the *NGL* and possibly the *PGL*. There were large enhancements in total number concentration especially for smaller particles (< 100 µm) in the *NGL* and *PGL*. In the *EAL* needles appeared aggregated although relatively limited data was collected to quantitatively describe this layer.

Acknowledgements

This work was funded by the NASA Earth Venture Suborbital-3 (EVS-3) program under grant NASA 80NSSC19K0355 (IMPACTS). All data is publicly available in the NASA EOSDID GHRC Archive: http://dx.doi.org/10.5067/IMPACTS/DATA101